

S.M. Adler-Golden, P. Conforti, M. Gagnon, P. Tremblay and M. Chamberland, Long-wave infrared surface reflectance spectra retrieved from Telops Hyper-Cam imagery, Proc. SPIE 9088, Algorithms and Technologies for Multispectral, Hyperspectral, and Ultraspectral Imagery XX, 90880U (June 13, 2014).

Copyright 2014, Society of Photo-Optical Instrumentation Engineers. One print or electronic copy may be made for personal use only. Systematic reproduction and distribution, duplication of any material in this paper for a fee or for commercial purposes, or modification of the content of the paper are prohibited.

doi:10.1117/12.2050446.

See next page.

Long-wave infrared surface reflectance spectra retrieved from Telops Hyper-Cam imagery

S. M. Adler-Golden^{*1}, P. Conforti¹, M. Gagnon², P. Tremblay² and M. Chamberland²

¹Spectral Sciences, Inc., 4 Fourth Avenue, Burlington, MA 01803

²Telops Inc., Québec, Qc, Canada G2E 6J5

ABSTRACT

Processing long-wave infrared (LWIR) hyperspectral imagery to surface emissivity or reflectance units via atmospheric compensation and temperature-emissivity separation (TES) affords the opportunity to remotely classify and identify solid materials with minimal interference from atmospheric effects. This paper describes an automated atmospheric compensation and TES method, called FLAASH[®]-IR (Fast Line-of-sight Atmospheric Analysis of Spectral Hypocubes – Infrared), and its application to ground-to-ground imagery taken with the Telops Inc. Hyper-Cam interferometric hyperspectral imager. The results demonstrate that clean, quantitative surface spectra can be obtained, even with highly reflective (low emissivity) objects such as bare metal and in the presence of some illumination from the surroundings. In particular, the atmospheric compensation process suppresses the spectral features due to atmospheric water vapor and ozone, which are especially prominent in reflected sky radiance.

Keywords: thermal infrared, hyperspectral, atmospheric compensation, correction, emissivity, reflectance, Hyper-Cam

1. INTRODUCTION

Hyperspectral imaging (HSI) technology provides a wealth of information for remotely identifying and characterizing surface materials and objects based on their spectral signatures. Long-wave and mid-wave infrared (L/MWIR) HSI sensors can yield both surface emissivity spectra and temperatures, provided that the corrupting effects of the atmosphere can be removed and the surface-leaving radiance factored into emissivity and Planck function components. The important atmospheric effects in the thermal infrared are absorption, thermal emission (path radiance), and reflected environmental illumination, which for upward-facing surfaces is dominated by skylight. Since precise knowledge of the atmospheric conditions is not generally available, the atmospheric description must be retrieved from the image itself. Removal of the atmospheric components is commonly called atmospheric compensation or correction, while the emissivity factorization is called temperature/emissivity separation (TES).

In general, atmospheric compensation methods for the L/MWIR are less well established and general than methods for the visible-shortwave IR region¹ because of the added complexity introduced by thermal emission. The atmospheric compensation is formally an underdetermined problem: the atmospheric parameters are usually unknown, and the emissivity spectrum for a given pixel is presumably unknown as well, so there are more unknowns than available spectral channels. Therefore, solutions to the atmospheric compensation and TES problems require some constraints on the spectrum and the atmospheric representation.

A variety of atmospheric compensation algorithms for the LWIR based on different assumptions and mathematical methods have recently been developed. Gillespie *et al.*² developed an algorithm that uses independent measurements of the atmospheric temperature and water vapor column densities. LWIR hyperspectral algorithms have been developed by Young *et al.*³ and Gu *et al.*⁴ that do not require ancillary information but do require the presence of a sufficient number of materials with unit emissivity in certain wavelength regions. Those two methods allow the retrieval of atmospheric transmission and path radiance information, but they do not treat the downwelling illumination and thus they are inaccurate for reflective (low emissivity) surfaces. Other algorithms rely on empirical relationships between emissivity spectral differences and mean or maximum emissivities.⁵ These methods work well for natural materials but fail for metallic and other man-made materials. Hernandez-Baquero and Schott⁶ developed a linear algebraic emissivity and temperature retrieval method that can be applied to arbitrary surfaces but is somewhat limited in the variety of materials and atmospheric conditions that can be handled. Boonmee *et al.*⁷ developed a complex algorithm that incorporates features from many earlier papers.

*adlergolden@spectral.com; phone 1 781 273-4770; fax 1 781 270-1161; www.spectral.com

A hyperspectral TES approach that is suitable for materials with arbitrary emissivity was developed by Borel⁸ based on the straightforward concept of maximizing emissivity spectral smoothness. A follow-up study by Ingram and Muse⁹ found this method to be robust to sensor noise and the presence of emissivity spectral features. Borel's approach was later extended to atmospheric retrieval along with TES.¹⁰ In this paper, we describe another smoothness-based automated atmospheric compensation and TES method, called FLAASH-IR (Fast Line-of-sight Atmospheric Analysis of Spectral Hypercubes – InfraRed), and its application to data taken with the Telops Inc. Hyper-Cam interferometric hyperspectral imager. We include an approximate treatment of the illumination of non-horizontal surfaces by the surrounding ground. The FLAASH-IR processing is found to almost entirely suppress the atmospheric features present in the radiance spectra, yielding surface reflectances that are consistent with laboratory measurements on similar materials.

2. ANALYSIS OVERVIEW

The LWIR spectral radiance measured by a sensor viewing objects on the ground can be written as

$$L_{\text{obs}}(\lambda) = B(T, \lambda)\varepsilon(\lambda)\tau(\lambda) + [1 - \varepsilon(\lambda)]L^{\downarrow}(\lambda) + L^{\uparrow}(\lambda) \quad (1)$$

where λ is wavelength, $\varepsilon(\lambda)$ is the composition- and temperature-averaged emissivity of the surface pixel, $\tau(\lambda)$ is the total (diffuse plus direct) transmittance between the surface and the sensor, $B(T, \lambda)$ is the surface Planck blackbody function at temperature T , $L^{\downarrow}(\lambda)$ is the incident illumination, and $L^{\uparrow}(\lambda)$ is the atmospheric path radiance. $L^{\uparrow}(\lambda)$ and $\tau(\lambda)$ are typically dominated by gases but may also include a scattering component. $L^{\downarrow}(\lambda)$ includes the atmospheric absorption between the surface and the sensor; i.e., it represents the at-sensor radiance originating from a hypothetical unit reflectance surface. $\tau(\lambda)$, $L^{\downarrow}(\lambda)$ and $L^{\uparrow}(\lambda)$ may be simulated for a given set of atmospheric properties using a radiation transport model such as MODTRAN[®].¹¹ The surface temperature, T , is effectively an emissivity-weighted average within each pixel. Eq. (1) is rigorous for Lambertian surfaces; for specular surfaces the emissivity and illumination quantities may be regarded as “effective.”

For hyperspectral sensors, the spectral channels are typically narrow enough that within-channel variations in emissivity and the blackbody function can be neglected. Therefore the atmospheric radiance and transmittance parameters in Eq. (1) are convolved with the wavelength response functions and assigned to their center wavelengths.

2.1 Temperature and Emissivity Separation (TES)

For a given model atmosphere defining the transmittance, path and illumination radiances, Eq. (1) leads to a family of emissivity spectrum solutions corresponding to a range of possible surface temperatures:

$$\varepsilon = (L - L^{\downarrow} - L^{\uparrow}) / (B(T)\tau - L^{\downarrow}) \quad (2)$$

The quantities in Eq. (2) are implicitly wavelength dependent.

According to the smooth-emissivity criterion, the most likely solution is the one with the least spectral fine structure. A useful measure of emissivity fine structure is the mean square residual between the emissivity spectrum and the same spectrum smoothed by taking a running average over some number of adjacent spectral channels, denoted as $\langle \varepsilon \rangle$. A better measure, which is adopted in FLAASH-IR, is obtained by inserting $\langle \varepsilon \rangle$ into Eq. (1) and taking the mean square of the difference between the computed radiance and the original data:

$$\sigma^2 = \underline{[L_{\text{obs}} - L(\langle \varepsilon \rangle)]^2} \quad (3)$$

where

$$L(\langle \varepsilon \rangle) = B(T) \langle \varepsilon \rangle \tau + (1 - \langle \varepsilon \rangle)L^{\downarrow} + L^{\uparrow} \quad (4)$$

and the underline denotes the running average. The TES is performed by finding the minimum of σ^2 with respect to temperature. An advantage of this measure is that it is uniformly weighted across all wavelengths, regardless of atmospheric optical depth. This allows one to include optically thick spectral regions, where the emissivity is poorly determined but there is valuable information for retrieving atmospheric parameters, as described in the next section. The unsmoothed emissivity spectrum from Eq. (2) rather than the smoothed spectrum is reported as the retrieval result in order to retain true spectral fine structure.

The smooth-emissivity criterion can be derived from the weaker assumption that emissivity structure is uncorrelated with atmospheric features. We write σ^2 as

$$\sigma^2 = \underline{D_{\text{tot}}}^2 = (\underline{D_e} + \underline{D_a})^2 = (\underline{D_e}^2) + (\underline{D_a}^2) + 2(\underline{D_e}\underline{D_a}) \quad (5)$$

where $D_{\text{tot}} = L_{\text{obs}} - L(\langle \epsilon \rangle)$, D_e is the spectral residual due to emissivity fine structure, and D_a is the spectral residual associated with imperfect atmospheric compensation (i.e., due to model error and/or surface temperature error). The third term accounts for correlation between D_e and D_a . D_e and D_a are vectors in the space of spectral channels, with a random relative orientation since their spectra are uncorrelated. If the number of channels is large, the space is of high dimension and probability favors a very small correlation term. Since $(\underline{D_e}\underline{D_a})$ is very small and $(\underline{D_e}^2)$ is constant, minimizing σ^2 effectively minimizes the mean square atmospheric compensation residual $(\underline{D_a}^2)$. Therefore accurate surface temperatures are obtainable even in the presence of substantial emissivity spectral structure D_e .

FLAASH-IR contains some refinements of the σ^2 calculation that reduce its sensitivity to sensor artifacts. Among the most serious problems are uncertainties in wavelength calibration and the instrument function. Several strategies are invoked to minimize this. One is to use a wide smoothing window of around $\sim 0.3 \mu\text{m}$ (typically ~ 7 channels), and another is to combine this with 3-channel averaging that is applied to both the unsmoothed and smoothed emissivities before taking the difference. These steps cause σ^2 to emphasize coarser spectral features that are less wavelength-sensitive. The TES generally benefits from restricting the spectral region of interest to the $\sim 9\text{-}10.2 \mu\text{m}$ region around the ozone band, whose presence in the surface spectrum directly correlates with reflectance. However, the full $\sim 8\text{-}13 \mu\text{m}$ atmospheric window region is used for atmosphere retrieval, discussed below, as the water vapor features it contains are needed to characterize the water column density and the lower atmospheric temperature.

2.2 Atmosphere and Emissivity Retrieval

The σ^2 minimization approach discussed above is also used to retrieve atmospheric parameters for the scene. We assume that the image dimensions are small enough that a single, homogenous atmosphere suffices. Radiation transport model calculations of $\tau(\lambda)$, $L^\downarrow(\lambda)$ and $L^\uparrow(\lambda)$ depend on the assumed atmospheric species and temperature profiles. The challenge is to devise a family of plausible and sufficiently varied trial atmospheres that can be specified with a small number of variables.

If we consider the $8\text{-}13 \mu\text{m}$ spectral region and a sensor located within a few km of the ground, the most prominent atmospheric species is water vapor, and the key variables for the transmittance and path emission are the column water vapor and the air temperature near the ground. In the absence of clouds, the sky downwelling illumination is composed primarily of water vapor emission, which is controlled by these same variables, plus ozone band emission from the upper atmosphere. The latter can be controlled by specifying the column ozone and/or the upper atmospheric temperature. Unless otherwise noted the sky is assumed to be cloud-free. Effects due to clouds, the ground, or other blackbody-like sources of illumination are discussed in the next section.

In FLAASH-IR a set of trial atmospheric spectra is calculated by specifying a three-dimensional grid of atmospheric parameters (e.g., surface air temperature, water vapor column density or relative humidity, and an ozone column density scale factor). The parameters are used to modify a built-in MODTRAN model atmosphere, which may be selected by latitude and season. A tabulation of $\tau(\lambda)$, $L^\uparrow(\lambda)$ and $L^\downarrow(\lambda)$ spectra (which we refer to as a Transmittance, Upwelling, Downwelling Look-Up Table, or TUD LUT) is derived from outputs of MODTRAN5. Polynomial fitting is used to interpolate the spectra between the grid points.

The best-fit atmosphere model is retrieved from selected pixel spectra by minimizing the total σ^2 with respect to both surface temperature and the atmospheric variables. The selected pixels, typically around 10-20, are chosen to be diverse in brightness and spectral shape, so that different temperatures and materials are represented. In contrast to most other atmospheric compensation methods, it is desirable to include low emissivity (reflective) materials, such as metals, as they provide atmospheric downwelling radiance information. The σ^2 minimization involves one-dimensional surface temperature searches for the selected pixels, which are embedded within a three (or more)-dimensional atmosphere search conducted using a downhill simplex method.¹² Finally, the retrieved atmosphere is used together with the one-dimensional search to derive surface temperature and emissivity (or reflectance, $r = 1 - \epsilon$) for the entire image.

Because the atmospheric radiance features are sharp, any wavelength miscalibration leads to atmospheric residuals in the emissivity spectra. FLAASH-IR provides an automated calibration option in which a wavelength shift and stretch and a resolution scaling factor are included in the atmosphere search and retrieved as part of the σ^2 minimization. The revised wavelength scale is output with the emissivity or reflectance image.

Further refinement of the results can be performed with a spectral “polishing” option. The method is a generalization of that employed in the HATCH visible-shortwave IR atmospheric compensation code¹³, where smoothed reflectance spectra are used to recalculate the atmospheric transmission from the radiation transport equation. In FLAASH-IR the smoothed emissivity spectra from the selected diverse pixels are used, and up to all three atmospheric components, $\tau(\lambda)$, $L^\uparrow(\lambda)$ and $L^\downarrow(\lambda)$, are recalculated using a least-squares method.

2.3 Enhanced Illumination Modeling

Improved modeling of the illumination $L^\downarrow(\lambda)$ can often be achieved by using a blend of clear sky illumination and a blackbody-like environmental radiance. That is, the clear sky illumination, weighted by f , representing an effective angular fraction of the sky hemisphere, is combined with a blackbody term weighted by $1-f$. This approach allows quantitative reflectances to be extracted from cloudy scenes, and can also compensate for emission from ground objects, which becomes important in horizontal and near-horizontal views. However, in the latter situation the sky fraction is dependent on surface orientation, so there is no single correct value for all surfaces in the scene. Inclusion of the blackbody radiance tends to have a minor effect on the shape of the reflectance spectrum, although the amplitude will vary. We demonstrate the latter point analytically in the approximation that the environmental and surface Planck functions are equal. In this case we replace L^\downarrow in Equation (1) with $L^{\downarrow'}$, given by

$$L^{\downarrow'} = fL^\downarrow + (1-f) [B(T)(1-r')\tau + L^\downarrow r'] \quad (6)$$

where $r = 1-\epsilon$ is the surface reflectance and r' is an effective environmental reflectance, included here for generality but typically very small (~ 0.1 or less). The result is a modified version of Equation (1),

$$L_{\text{obs}} = B(T)[1-fr-(1-f)rr']\tau + [fr+(1-f)rr']L^\downarrow + L^\uparrow \quad (7)$$

in which the retrieved reflectance is $fr+(1-f)rr'$. For $r' < 0.1$ the result is very close to fr . Thus, if the blackbody-like illumination is ignored the retrieved reflectance is reduced from its true value, r , by a factor equal to the clear sky fraction.

3. EXPERIMENT

The Telops Inc. Hyper-Cam LW is a portable imaging Fourier transform spectrometer operating in the 8-12 μm longwave infrared (LWIR) spectral range. The detector is a 320x256 PV-MCT focal plane array detector that can be windowed and formatted to fit the desired image size and to decrease the acquisition time. The pixel IFOV is 0.35 mrad, and spectral resolution is user selectable from 0.25 to 150 cm^{-1} . The Hyper-Cam LW has been used in several ground-based field campaigns, including the demonstration of standoff chemical agent detection. More recently, the Hyper-Cam has been integrated into an airplane to provide airborne measurement capabilities.

Here we present results from an outdoor experiment in which a variety of mineral samples and two flat panels were placed on the ground at a distance of 30 m from the sensor. Behind the sensor was a low building. The minerals include a quartz monocrystal and several silicates and carbonates; the panels are a near-blackbody black painted panel and a lightly sandblasted aluminum sheet. The panels were propped up to face the sensor and tipped slightly backward to reduce the influence of nearby ground illumination. Spectral radiance images of the scene were taken at 4 cm^{-1} resolution, unapodized.

Figure 1 shows a 100x320 pixel false color image generated using ENVI (Environment for Visualizing Images) software with square root scaling and some contrast enhancement. The image is free of obvious artifacts, such as striping, blurring or noise. The aluminum panel, the quartz monocrystal sample at far right and the fence in the background are very dark because of their low emissivities. The leaves are also fairly dark because of their relatively low temperature, within a few degrees of ambient.



Figure 1. Radiance image of the mineral scene in false color (RGB = 8.22, 9.52, 11.32 μm). Large rectangular panels are aluminum (left) and black painted (right). Green object at far left is a leafy branch. Dark line across the top is the bottom of a metal fence in the background.

FLAASH-IR was run on these data using a base US Standard model atmosphere, 1 cm^{-1} resolution MODTRAN calculations, and a spectral polishing option. The diverse pixels for the atmosphere retrieval were selected with the aid of an automated endmember code.¹⁴ A wide range of atmospheric water vapor was chosen initially and then narrowed down in a second iteration to achieve slightly better polynomial fits to the MODTRAN outputs. The results were output in units of reflectance versus wavelength for comparison with material library spectra provided in ENVI.

4. RESULTS

Our first result was obtained by ignoring non-sky illumination (i.e., $f=1$). Figure 2 shows the FLAASH-IR spectral reflectance image using the same color scheme and square root scaling as in Figure 1. In contrast to the thermal radiance image, the reflectance image has the qualitative appearance of a visible photograph, and we have found this to be typically the case with FLAASH-IR outputs. This is partly due to the similar reflectivities of some common materials, such as metals (high) and vegetation (low), across the visible and LWIR. In addition, in both wavelength regimes the reflectance image has similar sensitivity to surface orientation relative to the sky, with highlights and shadows appearing on surfaces that face upwards or downwards, respectively. Since sky illumination in the LWIR is diffuse, the visible analogue is an overcast sky.



Figure 2. FLAASH-IR reflectance image in the Figure 1 false color scheme.

A typical reflectance spectrum of the aluminum panel from this calculation is shown in the first panel in Figure 3. It is reasonably smooth and flat, and averages around 0.66. The actual reflectance of the panel is not known, but typical values for aluminum in the LWIR are between 0.8 and 0.95, depending on the surface roughness and degree of oxidation. Since the panel is in a near vertical orientation, we ascribe the smaller observed value to environmental illumination from the nearby ground and building.

Next, we performed a couple of additional calculations using less than full sky fractions to account for the environmental illumination. For simplicity this source was represented by a blackbody at 295K, selected to be somewhat below the likely surface temperatures to account for an average emissivity below unity. A reasonable reflectance for the aluminum panel, averaging around 0.85, was obtained using $f=0.8$. The spectrum is compared with that from the first calculation in Figure 3. In addition to having a higher average reflectance, the new spectrum is slightly flatter at the shorter wavelengths.

The remaining plots in Figure 3 show mineral spectra derived from the $f=0.8$ calculation along with laboratory spectra from the Johns Hopkins University infrared reflectance library.¹⁵ For the quartz monocrystal we show results for two pixels, one located on the brightest facet and another on a side facet. As the brightest facet appears to be sky-facing, we show the $f=1$ result for that pixel. Both results agree well with the most reflective of the library quartz spectra. For the other mineral samples only generic classifications (i.e., carbonates, silicates) are known, so we show library spectra within those mineral types that provide good matches.

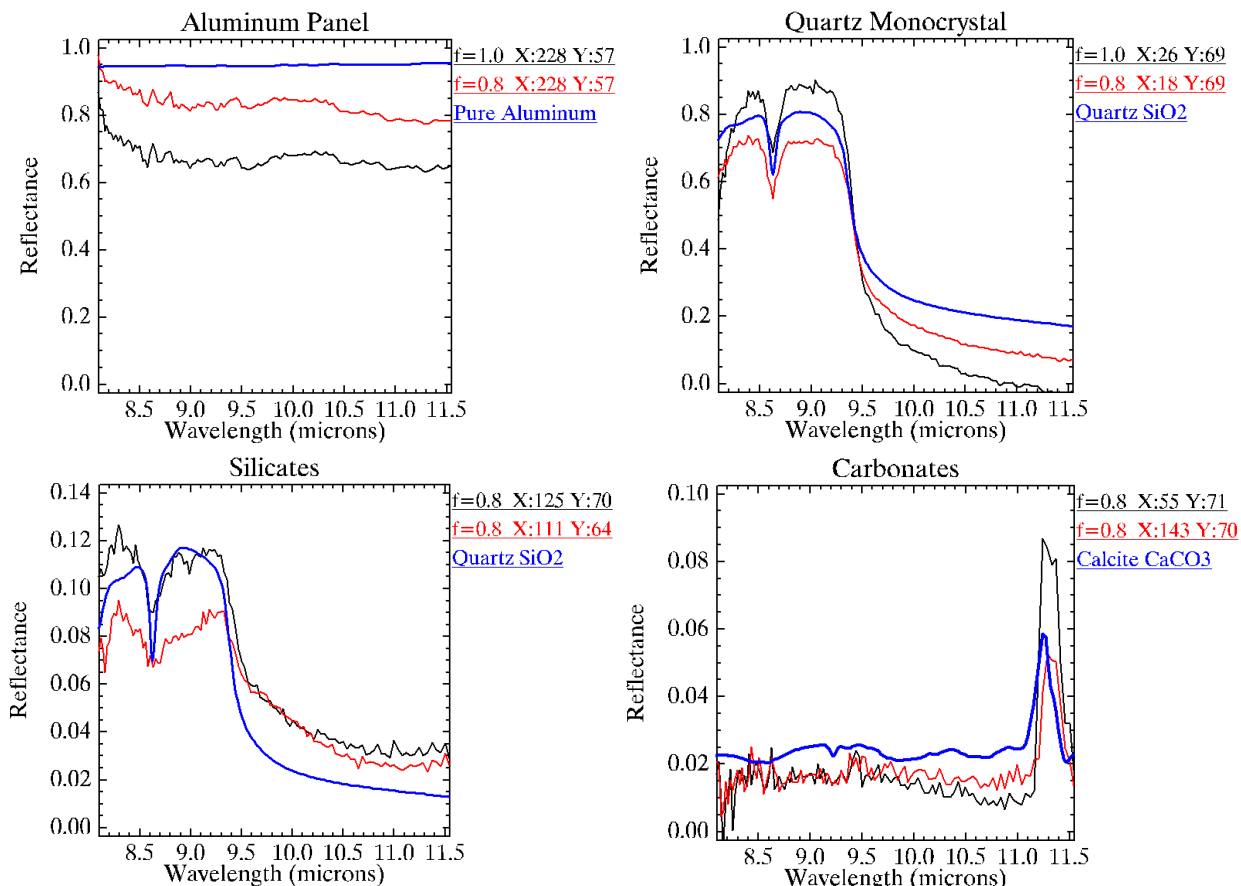


Figure 3. Derived reflectances for diverse scene materials (thin curves) and similar spectra from the JHU library (heavy curves). Assumed sky fraction values f and pixel coordinates x,y are noted.

Figure 4 compares corresponding reflectance and radiance spectra for these materials. The radiance spectra of the highly reflective quartz monocrystal and aluminum contain strong features from atmospheric water vapor and ozone. The ozone band originates from the sky downwelling illumination. In this experiment the water lines are also mainly from sky illumination, as the atmospheric transmission is very high (greater than 90% above 8.2 μm) at the 30 m standoff distance. All of these atmospheric features are almost completely removed in FLAASH-IR's conversion to spectral reflectance.

5. CONCLUSIONS

Processing LWIR hyperspectral imagery to reflectance units via atmospheric compensation and temperature-emissivity separation (TES) affords the opportunity to classify and identify solid materials with minimal interference from atmospheric effects. Other studies have demonstrated similar capabilities in natural scenes observed from the air, typically under dry, clear atmospheric conditions and with natural materials that are not highly reflective. This study, utilizing data from the Telops Hyper-Cam LW sensor and processing by the FLAASH-IR atmospheric compensation and TES code, shows that clean-looking surface reflectance or emissivity spectra can also be obtained in ground-to-ground (near-horizontal) observations, where there is significant illumination from the surrounding environment, and with

highly reflective objects including bare metal. In particular, FLAASH-IR performs well with the stressing combination of high reflectivity and moderately high spectral resolution (4 cm^{-1} , or around 1.6x better than that of SEBASS³), where prominent, sharp spectral structure originating from sky illumination is removed by the atmospheric compensation process.

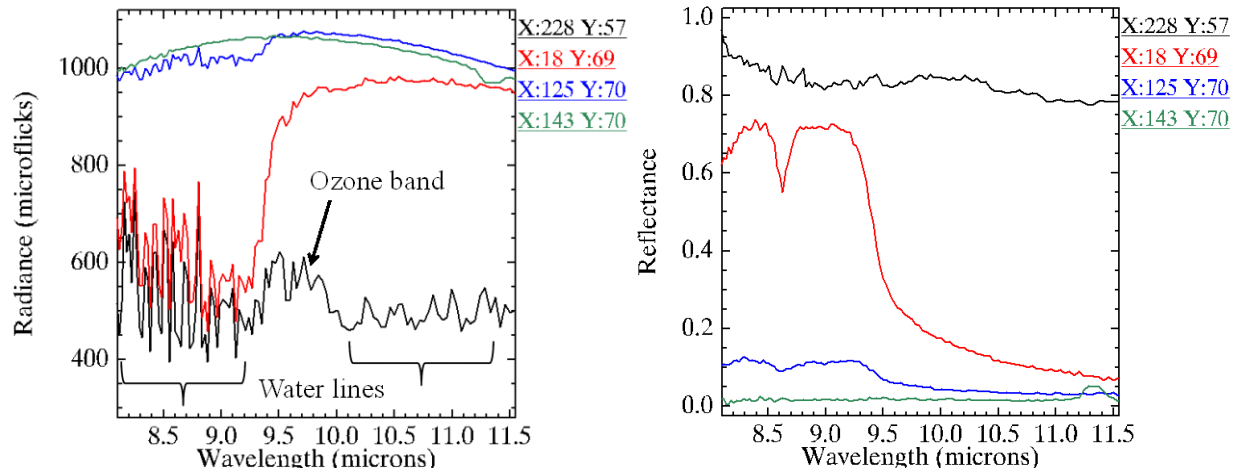


Figure 4. Comparison of spectral radiance (left) and derived reflectance (right) for the materials.

In this study as well as in other observations and radiation transport models, uncompensated illumination contributions from cloud or nearby surface emissions result in lower apparent reflectance values, although the reflectance spectrum shapes are reasonably preserved. While this is only a moderate effect in the data analyzed here, more severe reflectance signature reductions due to overcast weather or the presence of nearby tall objects significantly limit the utility of LWIR hyperspectral measurements.

ACKNOWLEDGEMENT

We thank Jeannette van den Bosch of the Air Force Research Laboratory for her valuable review of this manuscript.

REFERENCES

- [1] Matthew, M.W., S.M. Adler-Golden, A. Berk, G. Felde, G.P. Anderson, D. Gorodetzky, S. Paswaters and M. Shippert, "Atmospheric Correction of Spectral Imagery: Evaluation of the FLAASH Algorithm with AVIRIS Data," SPIE Proceedings, Algorithms and Technologies for Multispectral, Hyperspectral, and Ultraspectral Imagery IX, Vol. 5093, pp. 474-482 (2003).
- [2] Gillespie, A., S. Rokugawa, T. Matsunaga, J. S. Cothorn, S. Hook and A. B. Kahle, "A Temperature and Emissivity Separation Algorithm for Advanced Spaceborne Thermal Emission and Reflection Radiometer (ASTER) Images," IEEE Trans. Geosci. Remote Sens. 36, pp.1113-1126 (1998).
- [3] Young, S.J., B.R. Johnson and J. A. Hackwell, "An In-scene Method for Atmospheric Compensation of Thermal Hyperspectral Data," J. Geophys. Res. Atmospheres, Vol. 204, pp. ACH 14-1 – ACH 14-20 (2002).
- [4] Gu, D., A. R. Gillespie, A. B. Kahle, and F. D. Palluconi, "Autonomous Atmospheric Compensation of High Resolution Hyperspectral Thermal Infrared Remote-Sensing Imagery," IEEE Trans. Geosci. Remote Sens. 38, pp. 2557-2569 (2000).
- [5] Matsunaga, T., "An Emissivity-Temperature Separation Technique Based on an Empirical Relationship Between Mean and Range of Spectral Emissivity," Proc. 14th Japanese Conf. of Remote Sensing, pp. 47-48 (1993).

- [6] Hernandez-Baquero, E.D. and J. R. Schott, "Atmospheric compensation for surface temperature and emissivity separation," SPIE Proceedings, Algorithms for Multispectral, Hyperspectral, and Ultraspectral Imagery VI, Vol. 4049, pp. 400-410 (2000).
- [7] Boonmee, M., J.R. Schott and D.W. Messinger, "Land surface temperature and emissivity retrieval from thermal infrared hyperspectral imagery," Algorithms and Technologies for Multispectral, Hyperspectral, and Ultraspectral Imagery XII, Sylvia Shen and Paul Lewis, eds., Proc. SPIE 6233, 62331V (2006).
- [8] Borel, C.C., "Iterative Retrieval of Surface Emissivity and Temperature for a Hyperspectral Sensor," First JPL Workshop on Remote Sensing of Land Surface Emissivity, May 6-8, 1997, pp. 1-5.
- [9] Ingram, P.M. and A. H. Muse, "Sensitivity of Iterative Spectrally Smooth Temperature/Emissivity Separation to Algorithmic Assumptions and Measurement Noise," IEEE Trans. Geosci. Remote Sens. 39, pp. 2158-2167 (2001).
- [10] Borel, C.C., "ARTEMISS – an Algorithm to Retrieve Temperature and Emissivity from Hyper-Spectral Thermal Image Data," 28th Annual GOMACTech Conference, Hyperspectral Imaging Session, Tampa, FL, Los Alamos National Lab. Rpt. No. LA-UR-027907 (2003).
- [11] Berk, A., G.P. Anderson, P.K. Acharya, L.S. Bernstein, L. Muratov, J. Lee, M.J. Fox, S.M. Adler-Golden, J.H. Chetwynd, M.L. Hoke, R.B. Lockwood, T.W. Cooley and J.A. Gardner, "MODTRAN5: a Reformulated Atmospheric Band Model with Auxiliary Species and Practical Multiple Scattering Options," Proc. SPIE Int. Soc. Opt. Eng. 5655, 88 (2005).
- [12] Press, W.H., B.P. Flannery, S.A. Teukolsky, and W.T. Vetterling, "Numerical Recipes," 2nd edn., Cambridge University Press, Cambridge (1992).
- [13] Qu, Z., B.C. Kindel and A.F.H. Goetz, "The High Accuracy Atmospheric Correction for Hyperspectral Data (HATCH) model," IEEE Trans. Geosci. Remote Sens. 41, DOI:10.1109/TGRS.2003.813125 (2001).
- [14] Gruninger, J.H., A. J. Ratkowski and M. L. Hoke, "The Sequential Maximum Angle Convex Cone (SMACC) Endmember Model," SPIE Proceedings, Algorithms for Multispectral, Hyperspectral and Ultraspectral Imagery, Vol. 5425-1, Orlando FL (2004).
- [15] Johns Hopkins University spectral library, available from <<http://speclib.jpl.nasa.gov/>> (2006).